Precision Anisotropic Brush Polymers by Sequence Controlled Chemistry

Chaojian Chen,[†,‡] Katrin Wunderlich,[†] Debashish Mukherji,[†,§] Kaloian Koynov,[†] Astrid Johanna Heck,[†] Marco Raabe,[†,‡] Matthias Barz,[‖] George Fytas,[†,⊥] Kurt Kremer,[†] David Yuen Wah Ng,*[†] and Tanja Weil*[†,‡]

[†]Max Planck Institute for Polymer Research, Ackermannweg 10, 55128 Mainz, Germany
[‡]Ulm University, Albert-Einstein-Allee 11, 89081 Ulm, Germany
[§]Stewart Blusson Quantum Matter Institute, University of British Columbia, Vancouver V6T 1Z4, Canada
[‖]Johannes Gutenberg University Mainz, Duesbergweg 10-14, 55128 Mainz, Germany
[⊥]Institute of Electronic Structure and Laser, Foundation for Research and Technology, P.O. Box 1527, 71110 Heraklion, Greece

S *Supporting Information*

ABSTRACT: The programming of nanomaterials at molecular length-scales to control architecture and function represents a pinnacle in soft materials synthesis. Although elusive in synthetic materials, Nature has evolutionarily refined macromolecular synthesis with perfect atomic resolution across three-dimensional space that serves specific functions. We show that biomolecules, specifically proteins, provide an intrinsic macromolecular backbone for the construction of anisotropic brush polymers with monodisperse lengths via grafting-from strategy. Using human serum albumin as a model, its sequence was exploited to chemically transform a single cysteine, such that the expression of said functionality is asymmetrically placed along the backbone of the eventual brush polymer. This positional monofunctionalization strategy was connected with biotin−streptavidin interactions to demonstrate the capabilities for site-specific self-assembly to create higher ordered architectures. Supported by systematic experimental and computational studies, we envisioned that this macromolecular platform provides unique avenues and perspectives in macromolecular design for both nanoscience and biomedicine.
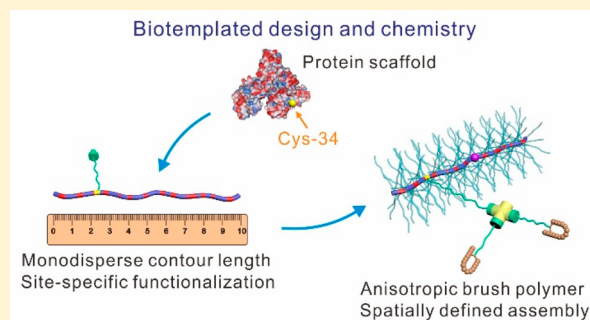
INTRODUCTION

Chemistry at the macromolecular level is often radically challenged by the exposure of target functional groups as they are inevitably subjected to the influences of structural conformation in solution. Although synthetic methods such as ultrafast click chemistry and bio-orthogonal reactions do alleviate these problems significantly,[1,2] the subject of conformational factors cannot be solved by fast reaction kinetics alone. The access toward a chemical moiety is dictated by numerous noncovalent intramolecular forces and is further amplified especially for any site-oriented chemistry. For synthetic macromolecules such as polymers, it is seemingly an unsurmountable task to map accessibility of each functional side chain due to its dispersity as well as the pseudorandom-ness of its sequence. Hence, the resolution of molecular engineering on polymers has been broadly restricted on a statistical basis despite impressive advances in controlled living polymerization methodologies.[3−5] Nonetheless, polymer-based methods have, in fact, contributed a fast-track route to probe different aspects of nanoscience, i.e., size, shape, and surfaces due to its facile synthesis.

In the repertoire of nanotechnology, the shape or anisotropy of an object was the most recent addition to the facet of nanoengineering, as their unique material properties as well as biological behavior have intrigued the community in both disciplines.[6] Among various anisotropic synthetic architectures, brush polymers constitute a dominant proportion where they have demonstrated unusual mechanical properties and rheological behavior[7−11] as well as being successfully employed as templates for the fabrication of nanotubes,[12,13] nanowires,[14] networks,[15] and nanoporous materials.[16] In biomedicine, wormlike brush polymers have been applied for tumor imaging and as delivery vehicles for therapeutics due to their unique pharmacokinetics.[17−19] In view of these broad applications, a deeper understanding would necessitate structure−function relationships with molecular information. However, pure polymer chemistry alone does not adequately resolve these recurring questions due to its limitations in providing accurate information on the distribution of chemical functionalities.
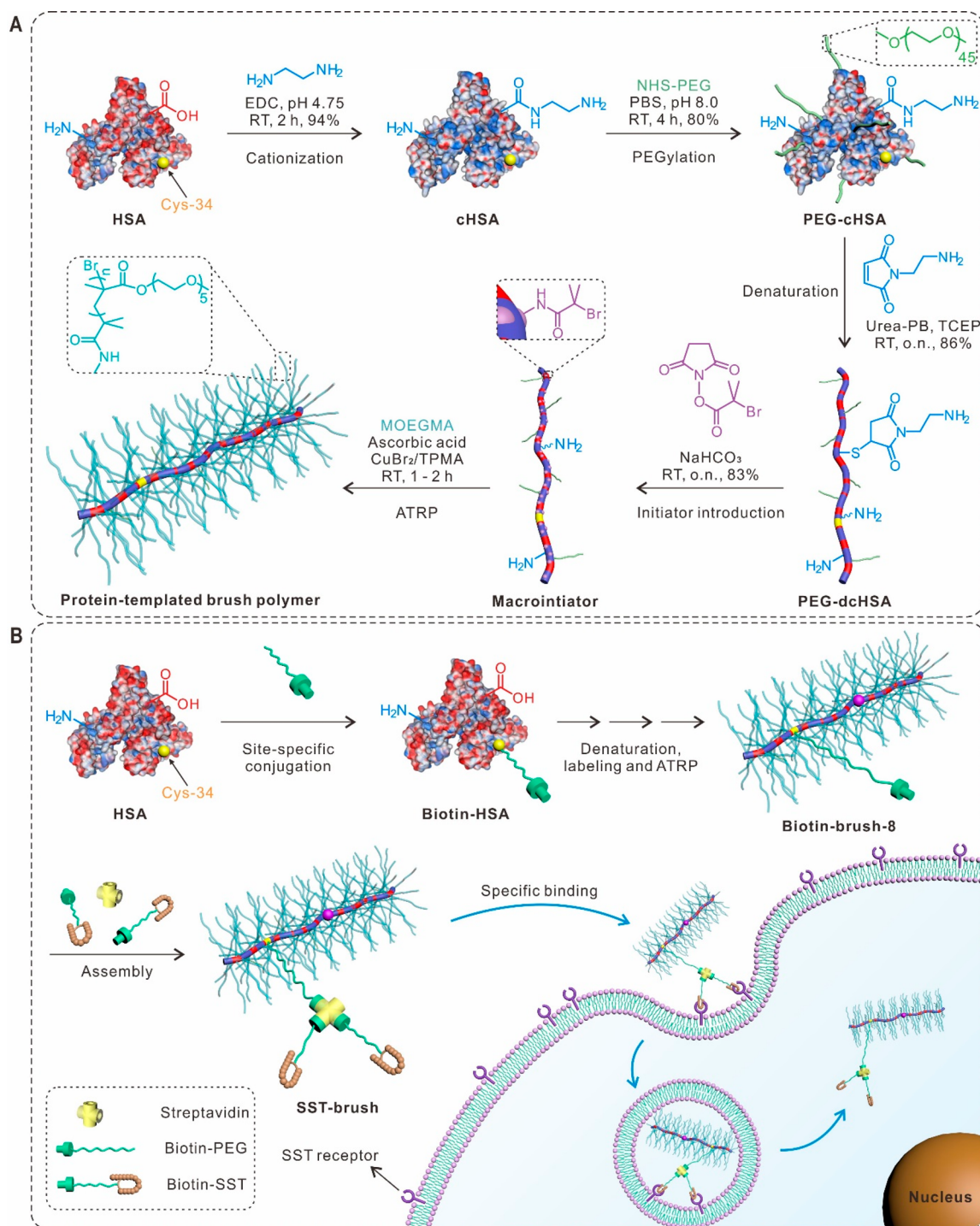
Figure 1. Synthesis and site-specific functionalization of protein-templated brush polymers. (A) Scheme for the synthesis of protein-templated brush polymers by grafting polymer chains from unfolded human serum albumin (HSA) via ATRP. (B) Site-specific conjugation of biotin-PEG to cysteine-34 (Cys-34) of HSA for preparation of the functional brush polymer (**biotin-brush-8**) with a spatially defined biotin group. The biotin group can be used as a versatile handle for the assembly with different functional objects in combination with the adapter protein streptavidin. For example, biotinylated somatostatin (biotin-SST) was introduced for mediating cellular uptake by receptor-mediated endocytosis.

Unlike synthetic chemistry, Nature produces biopolymers such as proteins in which the exact information on each atom's location on the polymer chain is known and invariable. We show herein that by tapping into the vast proteome in biology, the polypeptide chain of proteins is an extraordinary macromolecular backbone that presents far-reaching perspectives in the development of precision nanomaterials. Physically, proteins are monodispersed, and therefore, have absolute

lengths which can be tuned by simply choosing a desired protein class.[20] The exact sequence of amino acids is known easily from online databases allowing rational chemical design directly from its macromolecular blueprint. Hence, chemical modifications on side chains of lysines (−NH2), cysteines (−SH), and aspartic/glutamic acids (−COOH) result in well-positioned functionalities at specific loci along the polypeptide backbone. These modifications can be characterized by well-
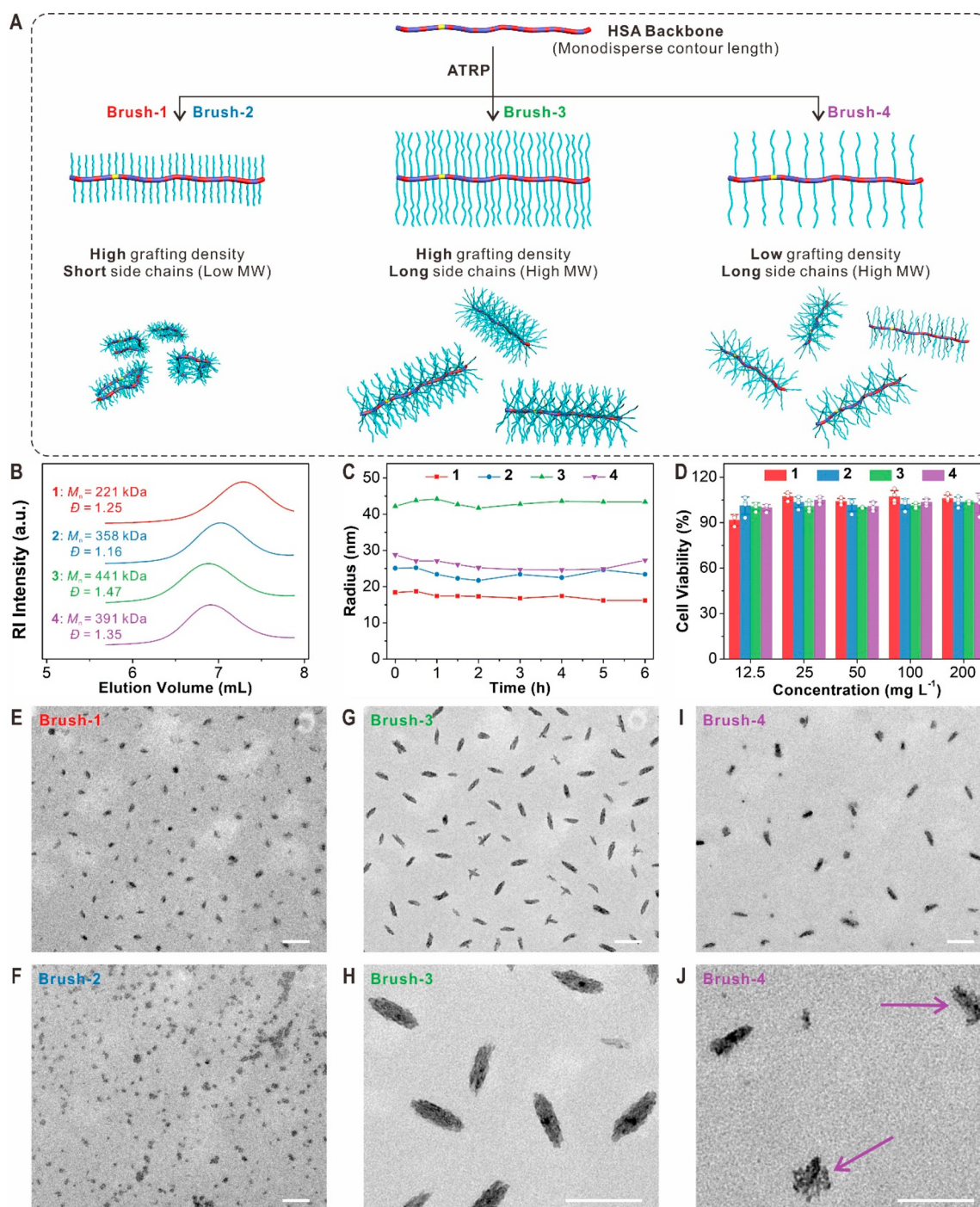
Figure 2. Characterization of **brush-1** to **brush-4**. (A) Schematic illustration of brush polymers synthesized with different grafting densities and side chain lengths from two macroinitiators. (B) GPC curves of **brush-1** to **brush-4**. (C) Size changes of **brush-1** to **brush-4** after mixing with the protease trypsin tracked by DLS. (D) Cell viability (24 h, 37 °C, 5% CO_2) test of **brush-1** to **brush-4** against A549 cells at various concentrations. (E) TEM image of **brush-1**. (F) TEM image of **brush-2**. (G) Low and (H) high magnification TEM images of **brush-3**. (I) Low and (J) high magnification TEM images of **brush-4**. Scale bars: 200 nm.

established mass fingerprinting technology unavailable to synthetic polymers. Furthermore, conformational perturbations affecting synthetic macromolecular chemistry are, conversely, minimized in proteins. Each protein molecule of the same type, as synthesized in biology, is folded identically in a rigid manner with a highly regular exposure of functional groups on its accessible surface. Importantly, by a subsequent denaturation of the globular protein in urea,[21,22] the originally

hidden side chains can become accessible and therefore be modified independently.[23,24]

To realize the implementation of Nature's technology in polymer chemistry, we use human serum albumin (HSA), a major blood plasma protein as a representative scaffold, on which a sequence of selective chemical and physical transformations are performed. These chemical reactions (e.g., functional group conversion, grafting "to" and "from" methods of polymer conjugation, supramolecular assembly) are

Table 1. Polymerization Conditions and Characterization of Brush-1 to Brush-4

category	parameter	brush-1	brush-2	brush-3	brush-4
polymerization	number of initiators	61	61	61	39
	monomer (vol %)	5%	10%	10%	10%
	time (h)	2	1	2	2
GPC[a]	M_n (kDa)	221	358	441	391
	M_w (kDa)	277	415	650	528
	M_p (kDa)	241	382	495	467
	Đ	1.25	1.16	1.47	1.35
TEM	length (nm)	56 ± 12	53 ± 13	139 ± 18	116 ± 24
	aspect ratio	1.83	1.51	2.85	2.51
light scattering	$R_g{}^b$ (nm)	19 ± 0.5	24 ± 0.5	32 ± 1	22 ± 1 (28)[d]
	$R_h{}^c$ (nm)	23 ± 0.4	30 ± 0.3	38 ± 1	37 ± 1
	R_g/R_h	0.83	0.8	0.84	0.59
	a (nm)	26	32	38	28 (35)[d]
	b (nm)	20	24	34	20 (29)[d]
	R_h^{*e} (nm)	22	27	35	23 (31)[d]

[a]Measured by GPC using deionized water containing 0.1 M NaNO₃ as the mobile phase and linear PEG standards for calibration. [b]Measured by SLS. [c]Measured by DLS in aqueous solution (1 mg mL⁻¹). [d]The numbers in parentheses correspond to the scaling prediction (inset of Figure S13). [e]Computed for ellipsoidal shape using the listed a and b values.

conducted on a single protein chain to show their compatibility as well as the broad applicability of the system. By taking advantage of how functional groups are exposed differently in the native and denatured forms of HSA and the order in which the above reactions are conducted, the protein backbone can provide a large chemical space for structural design. While simpler statistical "grafting to" approaches on denatured proteins have been performed by our group,[23,25] these conjugates lack structural definition and do not incorporate site specificity that takes full advantage of the protein sequence. Herein, we present the synthesis of an anisotropic molecular brush with monodispersed contour length while asymmetrically equipping the brush with a target function with atomic precision (specifically at cysteine-34). In this way, we would like to demonstrate that proteins can efficiently act as a molecularly ordered template to create large anisotropic nanoobjects with chemical functions at precise loci.

RESULTS AND DISCUSSION

Protein-Templated Brush Polymers. The amino-acid sequence and relative solvent accessibility of native human serum albumin (HSA) can be extracted from Uniprot database and PyMOL (Figure S1 and Table S1 in the Supporting Information, SI). At the macromolecular design stage, we allocated specific roles to different amino acid side chains for the synthesis of a brush polymer: (1) a high density of amine moieties of lysine side chains is necessary to graft polymers from the protein backbone to provide shape anisotropy (Figure 1A); and (2) a specific amino acid side chain such as cysteine-34 to serve as an orthogonal focal point for assembling complex functions (Figure 1B).

First, the potential of using a protein backbone for the brush polymer synthesis was investigated. HSA was cationized with ethylenediamine to convert the surface carboxylic acid groups into amino functionalities for the conjugation reactions at a later stage. Sequentially, approximately 32 polyethylene glycol (PEG, 2000 g mol⁻¹) chains were grafted onto cationized HSA (cHSA) using standard N-hydroxysuccinimide chemistry (Figure 1A). These chains were necessary to stabilize the protein backbone in the following denaturation step in which the PEG-cHSA was unfolded and linearized in 5 M urea-

phosphate buffer (urea-PB) in the presence of tris(2-carboxyethyl) phosphine hydrochloride (TCEP) as a mild reducing agent. The reduced thiols were capped with N-(2-aminoethyl)maleimide trifluoroacetate to prevent refolding as well as increasing, further, the number of reactive amino groups on the protein backbone. Subsequently, the resulting denatured polypeptide (PEG-dcHSA) was modified with 2-bromoisobutanoic acid N-hydroxysuccinimide ester in different stoichiometries to afford two HSA macroinitiators with varying initiator densities. The products were characterized by matrix-assisted laser desorption/ionization time-of-flight (MALDI-ToF) mass spectrometry to show the extent of modifications, on average 39 and 61 initiators, respectively (PEG-dcHSA-Br₃₉, PEG-dcHSA-Br₆₁) (Figure S2).

While the growth of polymers from native proteins has been developed extensively, particularly as functional polymer–protein conjugates,[26−30] the application of protein scaffolds in their denatured form opens new possibilities that have not been investigated before. We selected activators regenerated by electron transfer atom transfer radical polymerization (ARGET ATRP) for the "grafting from" strategy, which has been shown to be particular suitable for the synthesis of brush-like polymers of high molecular weights in aqueous media.[31−33] Oligo (ethylene glycol) methyl ether methacrylate (MOEG-MA, $M_n \approx 300$ g mol⁻¹) was polymerized in the presence of copper(II) bromide/tris(2-pyridylmethyl)amine (CuBr₂/TPMA) under deoxygenated and inert conditions. Thereafter, the brush polymer was isolated and purified by ultrafiltration using a Vivaspin 6 centrifugal concentrator.

To demonstrate the effects of different chain lengths and grafting densities, four brush polymers (denoted as **brush-1** to **brush-4**) were prepared from two macroinitiators by varying the monomer concentration and polymerization time (Figure 2A, Table 1). The formation of the brush polymers was confirmed by gel permeation chromatography (GPC) with peak molecular weights M_p between 241 and 495 kDa using linear PEG as calibration standards (Figure 2B). As the brush polymers were highly branched, an important consideration is that the molecular weight interpretation from GPC could very well be underestimated. Among all four different polymerization conditions, **brush-3**, which was grafted from PEG-
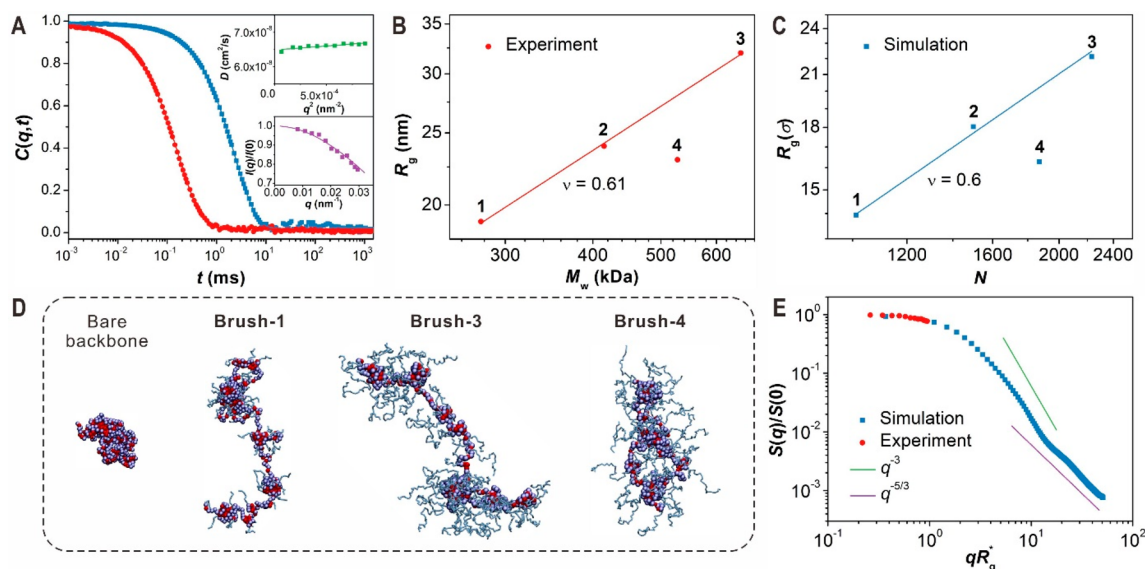
Figure 3. Light scattering and molecular simulation studies of **brush-1** to **brush-4** in solution. (A) Relaxation functions $C(q,t)$ for the translational diffusion dynamics in aqueous solution of **brush-3** (1 mg mL^{-1}) at 293 K at two scattering wave vectors (blue filled squares, $q = 0.008$ nm^{-1} and red filled circles, $q = 0.030$ nm^{-1}) represented by a single exponential decay (solid lines). Upper inset: The diffusion coefficient, D as a function of q^2 with the solid line indicating a linear representation. Lower inset: Normalized light scattering intensity $I(q)/I(0)$ as a function of q, where the solid line denotes the representation by the form factor of a solid prolate ellipsoid with semiaxes, $a = 38$ nm and $b = 34$ nm. (B and C) Chain gyration radius R_g as a function of overall molecular weight of brush polymers obtained from experiment (B) and simulation (C). A clear good solvent scaling is observed for both cases for the polymers with same grafting densities. (D) Simulation snapshots of the bare backbone and **brush-1**, **brush-3**, and **brush-4**. (E) Double-logarithmic plot of $S(q)/S(0)$ as a function of qR_g^*. Here, $S(0)$ is the total molecular weight of the brush polymer system, which is the total number of monomers in the simulation. Red filled circles and blue squares represent the experimental and simulated data, respectively.

dcHSA-Br$_{61}$ by applying the highest monomer concentration and longest polymerization time revealed a number-average molecular weight M_n of 441 kDa with a dispersity Đ of 1.47. Other variations by lowering the monomer concentrations or shortening polymerization time result in lower molecular weights and demonstrate significantly narrower dispersities. In comparison to other brush polymers grafted from pure synthetic polypeptide backbones of similar molecular weights, much larger dispersities in the range of 1.66−3.04 have been reported.[34,35] Moreover, these brush polymers were shelf stable and resistant toward rigorous proteolytic digestion by trypsin over 6 h, confirming the successful growth of a dense and protecting PEG shell (Figures 2C and S3). The cytotoxicity profile of these conjugates suggests their potential for drug delivery as these hybrids remain biocompatible to cells up to 0.2 g L^{-1} (Figure 2D).

Structural Anisotropy. The brush polymers (**brush-1** to **brush-4**) were imaged using transmission electron microscopy (TEM) to correlate the morphology with the grafted polymer chains (Figures 2E−J and S5−S9, Table 1). **Brush-1** synthesized with a lower monomer concentration (5%) and **brush-2** prepared with a shorter polymerization time (1 h) display elliptical and spherical shapes (Figures 2E,F). These observations strongly imply a plausible structural collapse as the shorter PMOEGMA side chains could not provide sufficient steric stabilization to linearize the backbone. Once the PMOEGMA side chains become longer, i.e., **brush-3** and **brush-4**, anisotropic worm-like structures were observed (Figure 2G−J). Statistically, the narrow size distributions of these elongated polymers serve as direct evidence that the 3D structure of HSA was successfully unfolded and stabilized in the extended form. However, it is interesting to note on **brush-4** that some spherical and irregular nanostructures coexisted as

well as some indications of a more spreaded PEG side chains (Figure 2J purple arrows). In order to investigate these morphologies without the influences of sample preparation in TEM conducted in the dry state, we reveal the structure of **brush-1** to **brush-4** in the absence of interactions in dilute solutions utilizing light scattering techniques.

Dynamic and static light scattering (DLS/SLS) experiments on dilute aqueous solutions of **brush-1** to **brush-4** yield size and shape information harnessing both the diffusion dynamics and the intensity dependence on the scattering wave vector (q). The relaxation functions $C(q,t)$ were virtually single exponential as depicted exemplarily for **brush-3** in Figure 3A suggesting monodisperse structures in all four systems (Figures S10−S12). The hydrodynamic radius R_h was calculated from the diffusion coefficient (at $q = 0$) for all four brush polymers. The value of R_h increases in the range 20 to 40 nm (Table 1) being significantly larger than the corresponding value, $R_h = 2$ nm, for the macroinitiator PEG-dcHSA-Br$_{61}$. For all four polymers, the light scattering intensity $I(q)$ displayed a q-dependence that led to the calculation of the radius of gyration R_g (Figure S11B). Both R_h and R_g, summarized in Table 1 (Figure S13), showed a positive correlation between their respective sizes in solution to the extent of polymerization and/or grafting densities. For **brush-1** to **brush-3**, the ratio R_g/R_h conforms to that of ellipsoid structures with values of this ratio ranging from 0.775 to 4.[36] Only for **brush-4**, R_g/R_h decreases below the limit, suggesting that the HSA core is more compact in this variation (Figure 3D). While the PMOEGMA chains increase R_h, the lower grafting density have a smaller effect on the R_g than for **brush-1** to **brush-3**, leading to a very small R_g/R_h of 0.59. Such a small value has been observed as well for PNIPAM microgels[37] or cross-linked polystyrene nanoparticles.[38] Consequently, to obtain further
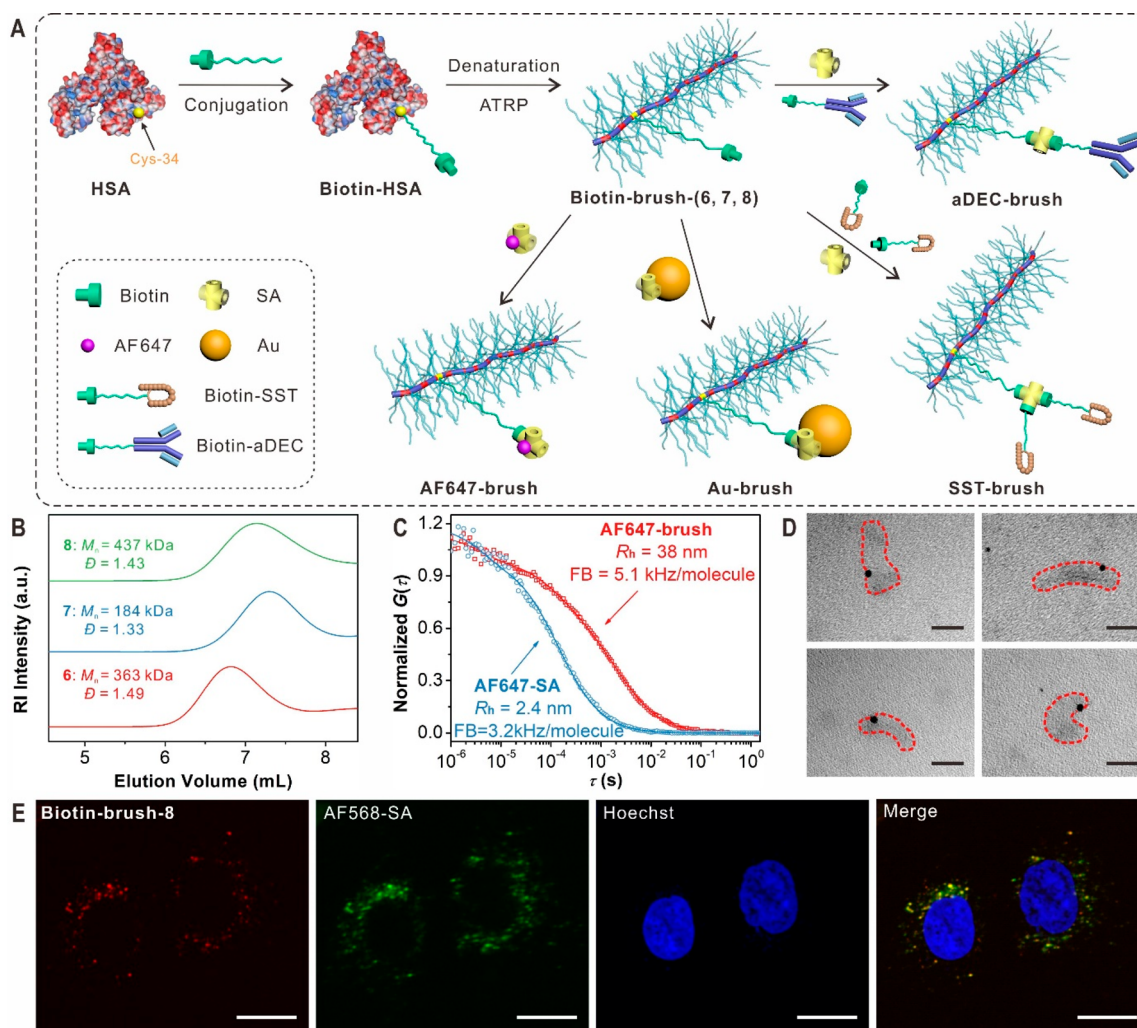
Figure 4. Brush polymers equipped with a biotin group for site-directed assembly. (A) Site-specific conjugation of biotin-PEG to Cys-34 of HSA for synthesis of brush polymers with a spatially defined biotin group, and their assembly with a spectrum of different functional objects: (1) AF647 labeled streptavidin (AF647-SA), (2) streptavidin-conjugated gold nanoparticles (Au-SA), (3) biotinylated somatostatin (biotin-SST) and streptavidin (SA), and (4) biotinylated aDEC205 antibody (biotin-aDEC) and SA. (B) GPC curves of biotin-functionalized brush polymers **biotin-brush-6**, **biotin-brush-7**, and fluorescent **biotin-brush-8**. (C) Normalized FCS autocorrelation curves measured in ~2 nM aqueous solutions of AF647-SA (blue circles) and its assembly with **biotin-brush-6** (AF647-brush, red squares). The solid lines represent the corresponding fits with eq S10. The fits yield the values of the hydrodynamic radius R_h and the fluorescence brightness (FB) of the studied species as indicated. (D) TEM images showing the assembly of **biotin-brush-7** with Au-SA. Scale bars: 20 nm. (E) Confocal laser scanning microscopy images showing the somatostatin-mediated cell uptake of **biotin-brush-8** after assembly with biotin-SST and AF568 labeled streptavidin (AF568-SA). The colocalization of **biotin-brush-8** and AF568-SA confirms the assembly process. Scale bars: 20 μm.

shape information, $I(q)$ is represented by the form factor of an ellipsoid with semiaxes a and b (Figures 3A and S13). The listed values suggest a prolate ($a > b$) ellipsoid. To prove the self-consistency of the data analysis, the computed hydrodynamic radii (R_h^*) of the ellipsoid using Perrin's theory[39] (SI) were compared against the experimental R_h values (Table 1). The agreement of these values from **brush-1** to **brush-3** represents unambiguous anisotropy in their solution structures. Nonetheless, it is interesting to note that for **brush-4**, a discrepancy (R_h^*, R_g, and R_g/R_h) (Figures 3B and S13) was observed. This might be attributed to differences in intramolecular packing of HSA and the grafted PMOEGMA chains in **brush-4**. Previously, significant change in the polymer packing due to the lower grafting density was also reported for tethered colloids.[40]

We seek to address the importance of how each macromolecule is intramolecularly packed by performing DLS/SLS

and molecular dynamic simulations using a generic bead-spring model (Figure 3B–E).[41] For this purpose, we have simulated a model brush polymer directly replicating the experiments in terms of backbone sequence/length, side chain lengths, and grafting densities (Table S2). The variations on the side chain lengths and grafting densities have a profound impact on the conformation of the brush polymers, whereas their resultant anisotropy as a prolate ellipsoid is consistent with DLS/SLS experimental observations. A closer inspection of Figure 3B,C illustrates that, for the same grafting density and varying side chain length (**brush-1** to **brush-3**), both SLS and simulation data show a good solvent scaling with the change in total molecular weight of the brush polymer. The deviation for **brush-4** is a result of lower grafting density which is consistent with literature.[42] We further illustrate simulation snapshots for three different systems (**brush 1**, **brush 3**, and **brush 4**) in comparison with a folded configuration of the bare protein

backbone (Figure 3D). More specifically, for **brush-1** and **brush-3**, a pearl necklace type configuration is observed, consisting of collapsed hydrophobic core and hairy hydrophilic side chains exposed to the solvent. Alternatively, because of the low grafting density, **brush-4** shows a more compact, rather distorted spherical configuration. It has been reported for uncharged brush polymers with flexible backbones that the lower the grafting density, the less elongated the main chain becomes.[42]

As the chain structures do not show the typical self-avoiding random walk configurations known for standard good solvent cases (Figures 3B,C), we further investigate this rather contradictory behavior. A quantity that best describes the overall conformation of a chain is the single chain structure factor $S(q)$. The simulation data of normalized structure factor $S(q)/S(0)$ is shown in Figure 3E for **brush-3**, with $S(0)$ being the total molecular weight of **brush-3**. The simulation result is in good agreement with the experimental data within the Gruinier regime (i.e., $q \rightarrow 0$). Note that the experimental data were obtained from SLS and therefore are only available for the long wavelength limit. Interestingly, we find that for small length scales (or large q values), **brush-3** behaves as if in a good solvent condition (represented by $q^{-5/3}$ power law) while globally it remains somewhat collapsed, showing a scaling q^{-3}. Note that if the chain was fully collapsed, as in the case of the bare backbone (Figure 3D), the system would show a perfect spherical scattering with the corresponding scaling q^{-4} instead. Although the system remains overall globular, it consists of rather large, good solvent blobs with sizes comparable to R_g (Figures 3B and Figure S16).

Site-Specific Functionalization and Assembly. While we have shown extensively that the monodispersity of proteins is a principle physical feature toward architectural design and anisotropy, the chemistry associated with its amino acid sequence is where diversification of functions takes root. To directly challenge the frontier of macromolecular chemistry, we designated the installation of a target functional moiety, precisely located on a single monomer unit in an asymmetrical position (No. 34 of 585 amino acids) along the protein backbone. The highlight would be that only one additional synthetic step is necessary by simply addressing an orthogonal functionality (Figure 4A).

Solvent accessible free thiols or disulfide bridges, characteristic of cysteines, are very often located on the surface of proteins and, in this case, HSA possesses a single thiol group in its native form. This thiol moiety is, without ambiguity, exactly located as the 34th amino acid, a cysteine (Cys-34), from the N-terminal of the protein. It can be projected that, after unfolding, any chemistry targeting Cys-34 would afford a function that is asymmetrically located along the 585-amino acid long protein backbone. Using this to our advantage, we performed a Michael reaction separately with Alexa Fluor 647 C$_2$ maleimide (AF647-MI) and maleimide end-capped biotin-PEG (biotin-PEG-MI) under chemoselective conditions on HSA (Figures S17−S18 and S24−S26). The respective monofunctionalized HSA (F-HSA, Biotin-HSA) follows the synthesis protocols for **brush-3** to afford the asymmetrically functionalized counterpart. By design, the inclusion of the fluorophore to afford **brush-5** represents a proof of concept and as a reporter for single particle fluorescence measurements (Figures S19−S21). However, the brush polymer equipped with a biotin-PEG extension aims to demonstrate the potential of the system to enable site-directed self-assembly (Figure 4A).

The brush polymer site-specifically functionalized with one AF647 group (**brush-5**) was characterized first with GPC (M_n = 409 kDa) as a quality control that the synthetic protocols are in line with **brush-3** (Figure S19). Visualization by TEM was similarly achieved and the expected anisotropic particles were observed (Figure S20). In order to probe the chemistry and the success of the concept, fluorescence correlation spectroscopy (FCS) was employed. While FCS operates on similar principles as DLS, it has the advantage to quantify and correlate single fluorophores with its connected nanostructure. Referenced against free AF647 (FB = 19 kHz/molecule), the fluorescence brightness of each molecule of **brush-5** (FB = 22 kHz/molecule) in combination with its measured hydrodynamic radius (R_h = 32 nm) demonstrated that each brush polymer is precisely equipped with a single fluorophore (Figures S22−S23).

Although the synthetic concepts were proven, the availability and its potential for functional capabilities (i.e., self-assembly) or ligand attachment cannot be demonstrated by a fluorophore alone. In this aspect, the biotin moiety enables a characteristic supramolecular interaction with the protein streptavidin, to showcase that the brush polymer can be further built-up with a defined spatial orientation. For this purpose, biotin-functionalized brush polymers **biotin-brush-6** (M_n = 363 kDa) and **biotin-brush-7** (M_n = 184 kDa, shorter side chains) were synthesized in anticipation of the potential steric constraints during the biotin/streptavidin binding event (Figure 4B). By adopting a similar approach using FCS, AF647-labeled streptavidin (AF647-SA) was used to quantify the assembly with **biotin-brush-6**. The increase in hydrodynamic radius from 2.4 to 38 nm monitored through the fluorophore suggests the successful binding of the small streptavidin (53 kDa) onto the brush polymer (Figure 4C). However, the fluorescence brightness indicates that, on average, slightly more than one streptavidin protein is bound to the brush polymer suggesting a minor presence of additional nonspecific adsorption of streptavidin.

We challenged the precision brush system further by the attachment of larger nanoobjects using streptavidin-conjugated gold nanoparticles (Au-SA, 5 nm) to explore its limitations as well as identify considerations from the design perspective. In addition, it provides better visualization of the binding event due to the different electron absorptivity between proteins and inorganic materials. The ligand/protein interaction was compared independently with both **biotin-brush-6** and **biotin-brush-7**. Due to the much larger steric requirements of the gold nanoparticle compared to free streptavidin protein, we observed successful binding events only with **biotin-brush-7** which has shorter side chains (Figure 4D). Notably, gold nanoparticles were observed to be positioned at the near-end of brush polymers which is consistent with the position of Cys-34 in the amino acid sequence of HSA. Hence, the TEM results suggest that the systematic built-up of higher ordered architectures can be tailored in a precise fashion using this technology.

To further demonstrate the broad applicability of the system, we expanded the system to assemble bioactive molecules. Here, we chose a hormonal targeting group, somatostatin, which targets the somatostatin receptor 2 (SSTR2) in cancer cells (Figure 1B). Using biotinylated somatostatin (biotin-SST) synthesized using an existing protocol,[43] the assembly consist of biotinylated fluorescent brush polymer **biotin-brush-8** (Figures S27), biotin-SST and

streptavidin (1:2:1 molar ratio). The afforded construct (500 nM) was incubated with A549 cells for 24 h where the cellular uptake was monitored with confocal laser scanning microscopy (Figure S29). In this experiment, somatostatin-mediated uptake was observed compared to the **biotin-brush-8**/streptavidin as the control. Fluorescence microscopy studies at 2 h, 6, and 24 h showed time dependent cellular uptake of the somatostatin functionalized brush (Figure S29). While receptor-mediated pathways generally possess faster uptake kinetics, we postulate that the slower internalization could be due to the large size and highly dense PEG brush. As a further confirmation, colocalization studies with an additional fluorescent label on streptavidin (AF568-SA) showed that the construct remains largely intact during the internalization process (Figures 4E and S30). As a final test to widen the biological relevance, we replace biotin-SST with biotinylated aDEC (biotin-aDEC), a model antibody, to show that the platform allows the assembly of both small peptides as well as a significantly larger protein. Here, we perform an SDS-PAGE and a Western blot to show the successful assembly process of both the somatostatin/antibody conjugated brush (Figures S31 and S32). Therefore, we have demonstrated that brush polymers site-specifically functionalized with a biotin group can be used as a powerful and versatile platform for assembly with a wide variety of functional entities.

CONCLUSIONS

In summary, a unique synthetic framework exploiting the architecture of proteins to construct precision anisotropic brush polymers was presented, along with a strong emphasis on its innate monodispersity and sequence controlled chemistry. The facile engineering of chemical strategies toward the control of size, contour lengths, and anisotropy was shown by simply varying (1) the initiator density on the polypeptide backbone, or (2) the polymerization conditions such as monomer concentration and polymerization time. In particular, a distinct chemical function was introduced onto an absolute position located asymmetrically along the polypeptide backbone which has, to the best of our knowledge, not been achieved before for other synthetic brush polymer systems. By exploiting this specific handle, we show its broad potential in assembling unique macromolecular conjugates from both material and biological perspectives. It should be noted that bioorthogonal chemical handles can be incorporated into any position of protein backbones through genetical engineering methods, therefore it is possible to stoichiometrically functionalize brush polymers with desired functions.

Collectively, the capacity of this platform is multiplicative in that each aspect including the backbone, chemical strategy, or polymerization techniques and design can be postulated to expand far greater than those explored within this study. Likewise, it is also conceivable to overcome the limitations presented within this study by varying the aforementioned factors. In perspective, by developing a methodical and extensive evaluation of this technology, we seek to stimulate exciting synergy with the available toolbox for site-selective protein chemistry and achieve molecular programming at the nanoscale.

ASSOCIATED CONTENT

Ⓢ Supporting Information

The Supporting Information is available free of charge at https://pubs.acs.org/doi/10.1021/jacs.9b10491.

Experimental details, characterization techniques, simulation details and further analysis, supplementary data, and discussion (PDF)

AUTHOR INFORMATION

Corresponding Authors
*david.ng@mpip-mainz.mpg.de
*weil@mpip-mainz.mpg.de

ORCID Ⓘ
Chaojian Chen: 0000-0002-2588-2447
Katrin Wunderlich: 0000-0002-8096-7427
Debashish Mukherji: 0000-0002-6242-1754
Kaloian Koynov: 0000-0002-4062-8834
Marco Raabe: 0000-0002-3677-6615
Matthias Barz: 0000-0002-1749-9034
Kurt Kremer: 0000-0003-1842-9369
David Yuen Wah Ng: 0000-0002-0302-0678
Tanja Weil: 0000-0002-5906-7205

Notes
The authors declare no competing financial interest.

REFERENCES

(1) Ouchi, M.; Badi, N.; Lutz, J. F.; Sawamoto, M. Single-chain technology using discrete synthetic macromolecules. *Nat. Chem.* **2011**, *3*, 917.

(2) Schmidt, B. V. K. J.; Fechler, N.; Falkenhagen, J.; Lutz, J. F. Controlled folding of synthetic polymer chains through the formation of positionable covalent bridges. *Nat. Chem.* **2011**, *3*, 234.

(3) Wang, J. S.; Matyjaszewski, K. Controlled living radical polymerization - atom-transfer radical polymerization in the presence of transition-metal complexes. *J. Am. Chem. Soc.* **1995**, *117*, 5614.

(4) Matyjaszewski, K.; Xia, J. H. Atom transfer radical polymerization. *Chem. Rev.* **2001**, *101*, 2921.

(5) Chiefari, J.; Chong, Y. K.; Ercole, F.; Krstina, J.; Jeffery, J.; Le, T. P. T.; Mayadunne, R. T. A.; Meijs, G. F.; Moad, C. L.; Moad, G.; Rizzardo, E.; Thang, S. H. Living free-radical polymerization by reversible addition-fragmentation chain transfer: The RAFT process. *Macromolecules* **1998**, *31*, 5559.

(6) Thorkelsson, K.; Bai, P.; Xu, T. Self-assembly and applications of anisotropic nanomaterials: A review. *Nano Today* **2015**, *10*, 48.

(7) Verduzco, R.; Li, X.; Pesek, S. L.; Stein, G. E. Structure, function, self-assembly, and applications of bottlebrush copolymers. *Chem. Soc. Rev.* **2015**, *44*, 2405.

(8) Sheiko, S. S.; Sumerlin, B. S.; Matyjaszewski, K. Cylindrical molecular brushes: Synthesis, characterization, and properties. *Prog. Polym. Sci.* **2008**, *33*, 759.

(9) Feng, C.; Li, Y. J.; Yang, D.; Hu, J. H.; Zhang, X. H.; Huang, X. Y. Well-defined graft copolymers: from controlled synthesis to multipurpose applications. *Chem. Soc. Rev.* **2011**, *40*, 1282.

(10) Vatankhah-Varnosfaderani, M.; Daniel, W. F. M.; Everhart, M. H.; Pandya, A. A.; Liang, H. Y.; Matyjaszewski, K.; Dobrynin, A. V.; Sheiko, S. S. Mimicking biological stress-strain behaviour with synthetic elastomers. *Nature* **2017**, *549*, 497.

(11) Daniel, W. F. M.; Burdynska, J.; Vatankhah-Varnoosfaderani, M.; Matyjaszewski, K.; Paturej, J.; Rubinstein, M.; Dobrynin, A. V.; Sheiko, S. S. Solvent-free, supersoft and superelastic bottlebrush melts and networks. *Nat. Mater.* **2016**, *15*, 183.

(12) Huang, K.; Rzayev, J. Well-defined organic nanotubes from multicomponent bottlebrush copolymers. *J. Am. Chem. Soc.* **2009**, *131*, 6880.

(13) Mullner, M.; Yuan, J. Y.; Weiss, S.; Walther, A.; Fortsch, M.; Drechsler, M.; Muller, A. H. E. Water-soluble organo-silica hybrid nanotubes templated by cylindrical polymer brushes. *J. Am. Chem. Soc.* **2010**, *132*, 16587.

(14) Yuan, J. Y.; Xu, Y. Y.; Walther, A.; Bolisetty, S.; Schumacher, M.; Schmalz, H.; Ballauff, M.; Muller, A. H. E. Water-soluble organo-silica hybrid nanowires. *Nat. Mater.* **2008**, *7*, 718.

(15) Wu, D. C.; Nese, A.; Pietrasik, J.; Liang, Y. R.; He, H. K.; Kruk, M.; Huang, L.; Kowalewski, T.; Matyjaszewski, K. Preparation of polymeric nanoscale networks from cylindrical molecular bottle-brushes. *ACS Nano* **2012**, *6*, 6208.

(16) Bolton, J.; Bailey, T. S.; Rzayev, J. Large pore size nanoporous materials from the self-assembly of asymmetric bottlebrush block copolymers. *Nano Lett.* **2011**, *11*, 998.

(17) Fouz, M. F.; Mukumoto, K.; Averick, S.; Molinar, O.; McCartney, B. M.; Matyjaszewski, K.; Armitage, B. A.; Das, S. R. Bright fluorescent nanotags from bottlebrush polymers with DNA-tipped bristles. *ACS Cent. Sci.* **2015**, *1*, 431.

(18) Luo, H. Y.; Szymusiak, M.; Garcia, E. A.; Lock, L. L.; Cui, H. G.; Liu, Y.; Herrera-Alonso, M. Solute-triggered morphological transitions of an amphiphilic heterografted brush copolymer as a single-molecule drug carrier. *Macromolecules* **2017**, *50*, 2201.

(19) Sowers, M. A.; McCombs, J. R.; Wang, Y.; Paletta, J. T.; Morton, S. W.; Dreaden, E. C.; Boska, M. D.; Ottaviani, M. F.; Hammond, P. T.; Rajca, A.; Johnson, J. A. Redox-responsive branched-bottlebrush polymers for in vivo MRI and fluorescence imaging. *Nat. Commun.* **2014**, *5*, 5460.

(20) Yang, J.; Gitlin, I.; Krishnamurthy, V. M.; Vazquez, J. A.; Costello, C. E.; Whitesides, G. M. Synthesis of monodisperse polymers from proteins. *J. Am. Chem. Soc.* **2003**, *125*, 12392.

(21) Wu, Y. Z.; Chakrabortty, S.; Gropeanu, R. A.; Wilhelmi, J.; Xu, Y.; Er, K. S.; Kuan, S. L.; Koynov, K.; Chan, Y.; Weil, T. pH-responsive quantum dots via an albumin polymer surface coating. *J. Am. Chem. Soc.* **2010**, *132*, 5012.

(22) Wu, Y. Z.; Pramanik, G.; Eisele, K.; Weil, T. Convenient approach to polypeptide copolymers derived from native proteins. *Biomacromolecules* **2012**, *13*, 1890.

(23) Wu, Y. Z.; Ermakova, A.; Liu, W. N.; Pramanik, G.; Vu, T. M.; Kurz, A.; McGuinness, L.; Naydenov, B.; Hafner, S.; Reuter, R.; Wrachtrup, J.; Isoya, J.; Fortsch, C.; Barth, H.; Simmet, T.; Jelezko, F.; Weil, T. Programmable biopolymers for advancing biomedical applications of fluorescent nanodiamonds. *Adv. Funct. Mater.* **2015**, *25*, 6576.

(24) Ng, D. Y. W.; Wu, Y. Z.; Kuan, S. L.; Weil, T. Programming supramolecular biohybrids as precision therapeutics. *Acc. Chem. Res.* **2014**, *47*, 3471.

(25) Wu, Y. Z.; Ihme, S.; Feuring-Buske, M.; Kuan, S. L.; Eisele, K.; Lamla, M.; Wang, Y. R.; Buske, C.; Weil, T. A core-shell albumin copolymer nanotransporter for high capacity loading and two-step release of doxorubicin with enhanced anti-leukemia activity. *Adv. Healthcare Mater.* **2013**, *2*, 884.

(26) Bontempo, D.; Maynard, H. D. Streptavidin as a macroinitiator for polymerization: In situ protein-polymer conjugate formation. *J. Am. Chem. Soc.* **2005**, *127*, 6508.

(27) Cobo, I.; Li, M.; Sumerlin, B. S.; Perrier, S. Smart hybrid materials by conjugation of responsive polymers to biomacromole-cules. *Nat. Mater.* **2015**, *14*, 143.

(28) De, P.; Li, M.; Gondi, S. R.; Sumerlin, B. S. Temperature-regulated activity of responsive polymer-protein conjugates prepared by grafting-from via RAFT polymerization. *J. Am. Chem. Soc.* **2008**, *130*, 11288.

(29) Heredia, K. L.; Bontempo, D.; Ly, T.; Byers, J. T.; Halstenberg, S.; Maynard, H. D. In situ preparation of protein - "Smart" polymer conjugates with retention of bioactivity. *J. Am. Chem. Soc.* **2005**, *127*, 16955.

(30) Lucon, J.; Qazi, S.; Uchida, M.; Bedwell, G. J.; LaFrance, B.; Prevelige, P. E.; Douglas, T. Use of the interior cavity of the P22 capsid for site-specific initiation of atom-transfer radical polymerization with high-density cargo loading. *Nat. Chem.* **2012**, *4*, 781.

(31) Averick, S.; Simakova, A.; Park, S.; Konkolewicz, D.; Magenau, A. J. D.; Mehl, R. A.; Matyjaszewski, K. ATRP under biologically relevant conditions: grafting from a protein. *ACS Macro Lett.* **2012**, *1*, 6.

(32) Oh, J. K.; Perineau, F.; Charleux, B.; Matyjaszewski, K. AGET ATRP in water and inverse miniemulsion: a facile route for preparation of high-molecular-weight biocompatible brush-like polymers. *J. Polym. Sci., Part A: Polym. Chem.* **2009**, *47*, 1771.

(33) Jakubowski, W.; Matyjaszewski, K. Activator generated by electron transfer for atom transfer radical polymerization. *Macromolecules* **2005**, *38*, 4139.

(34) Liu, Y.; Chen, P.; Li, Z. B. Molecular bottlebrushes with polypeptide backbone prepared via ring-opening polymerization of NCA and ATRP. *Macromol. Rapid Commun.* **2012**, *33*, 287.

(35) Lahasky, S. H.; Lu, L.; Huberty, W. A.; Cao, J. B.; Guo, L.; Garno, J. C.; Zhang, D. H. Synthesis and characterization of thermo-responsive polypeptoid bottlebrushes. *Polym. Chem.* **2014**, *5*, 1418.

(36) Schärtl, W. *Light Scattering from Polymer Solutions and Nanoparticle Dispersions*; Springer: Berlin/Heidelberg, 2007.

(37) Senff, H.; Richtering, W. Temperature sensitive microgel suspensions: Colloidal phase behavior and rheology of soft spheres. *J. Chem. Phys.* **1999**, *111*, 1705.

(38) Martin, H. J.; White, B. T.; Scanlon, C. J.; Saito, T.; Dadmun, M. D. Tunable synthetic control of soft polymeric nanoparticle morphology. *Soft Matter* **2017**, *13*, 8849.

(39) Zhao, J. Q.; Pearce, E. M.; Kwei, T. K.; Jeon, H. S.; Kesani, P. K.; Balsara, N. P. Micelles formed by a model hydrogen-bonding block-copolymer. *Macromolecules* **1995**, *28*, 1972.

(40) Cang, Y.; Reuss, A. N.; Lee, J.; Yan, J. J.; Zhang, J. N.; Alonso-Redondo, E.; Sainidou, R.; Rembert, P.; Matyjaszewski, K.; Bockstaller, M. R.; Fytas, G. Thermomechanical properties and glass dynamics of polymer-tethered colloidal particles and films. *Macromolecules* **2017**, *50*, 8658.

(41) Kremer, K.; Grest, G. S. Dynamics of entangled linear polymer melts - a molecular-dynamics simulation. *J. Chem. Phys.* **1990**, *92*, 5057.

(42) Kikuchi, M.; Nakano, R.; Jinbo, Y.; Saito, Y.; Ohno, S.; Togashi, D.; Enomoto, K.; Narumi, A.; Haba, O.; Kawaguchi, S. Graft density dependence of main chain stiffness in molecular rod brushes. *Macromolecules* **2015**, *48*, 5878.

(43) Wang, T.; Wu, Y. Z.; Kuan, S. L.; Dumele, O.; Lamla, M.; Ng, D. Y. W.; Arzt, M.; Thomas, J.; Mueller, J. O.; Barner-Kowollik, C.; Weil, T. A disulfide intercalator toolbox for the site-directed modification of polypeptides. *Chem. - Eur. J.* **2015**, *21*, 228.